Jamming and percolation of linear *k*-mers on honeycomb lattices

G. A. Iglesias Panuska, P. M. Centres, and A. J. Ramirez-Pastor*
Departamento de Física, Instituto de Física Aplicada, Universidad Nacional de San Luis-CONICET, Ejército de los Andes 950, D5700HHW, San Luis, Argentina

(Received 18 June 2020; accepted 25 August 2020; published 14 September 2020)

Numerical simulations and finite-size scaling analysis have been performed to study the jamming and percolation behavior of elongated objects deposited on two-dimensional honeycomb lattices. The depositing particle is modeled as a linear array of length k (so-called k-mer), maximizing the distance between first and last monomers in the chain. The separation between k-mer units is equal to the lattice constant. Hence, k sites are occupied by a k-mer when adsorbed onto the surface. The adsorption process starts with an initial configuration, where all lattice sites are empty. Then, the sites are occupied following a random sequential adsorption mechanism. The process finishes when the jamming state is reached and no more objects can be deposited due to the absence of empty site clusters of appropriate size and shape. Jamming coverage $\theta_{j,k}$ and percolation threshold $\theta_{c,k}$ were determined for a wide range of values of k ($2 \leqslant k \leqslant 128$). The obtained results shows that (*i*) $\theta_{j,k}$ is a decreasing function with increasing k, being $\theta_{j,k\to\infty} = 0.6007(6)$ the limit value for infinitely long k-mers; and (*ii*) $\theta_{c,k}$ has a strong dependence on k. It decreases in the range $2 \leqslant k < 48$, goes through a minimum around $k = 48$, and increases smoothly from $k = 48$ up to the largest studied value of $k = 128$. Finally, the precise determination of the critical exponents ν, β, and γ indicates that the model belongs to the same universality class as 2D standard percolation regardless of the value of k considered.

DOI: 10.1103/PhysRevE.102.032123

I. INTRODUCTION

Irreversible adsorption of extended objects is currently a very active field of research in surface science and statistical mechanics. The model appears to offer a good description of a great variety of complex surface processes such as adsorption of large molecules on solid substrates [1–3], particles deposited on cell membranes [4], latex spheres on a silica surface [5,6], etc. However, phenomena associated to irreversible adsorption, such as jamming and percolation, have been attractive and important topics in statistical physics for a long time [7–20]. In the case of percolation theory, the phase transition involved in the process can be described in terms of an usual second-order phase transition. This mapping to critical phenomena made percolation a full part of the theoretical framework of collective phenomena and statistical physics [21–24].

In the simplest case of irreversible adsorption, objects are deposited sequentially at random positions onto a lattice. Any trial leading to overlap with a previously placed object is rejected; and this process continues until no further particles may be placed due to the absence of free space of appropriate size and shape. Such processes are called random sequential adsorption (RSA) processes [7,25–28], and a quantity of central interest in RSA studies is the maximum fraction of extended objects that can be deposited on the lattice (jamming coverage).

However, one of the first results in percolation theory is that, depending on the lattice, there exists a minimum concentration of elements (sites or bonds) above which a cluster of occupied elements spans from one side of the lattice to the other. This minimum concentration of elements is named percolation threshold and determines a second-order phase transition in the system.

In some applications one may want that percolation dominates (i.e., communications), in others one may prefer that jamming dominates and percolation is suppressed at an early stage (i.e., forest fires). Thus, the competition between percolation threshold and jamming coverage is a field of great interest that has been addressed by various authors. In the case of linear k-mers on 2D lattices, which is the topic of this paper, the problem has been widely studied in the literature for square [8–14] and triangular [15–20] geometries.

In the case of straight rigid k-mers on square lattices, it was found that: (i) the limit coverage $\theta_{j,k}$ monotonically decreases with k, following a function $\theta_{j,k} = 0.660(2) + 1.071/k - 3.47/k^2$, where 0.660(2) represents the jamming concentration by infinitely long k-mers [8]; (ii) the percolation threshold is a nonmonotonic function of the size k: it decreases for small k sizes, goes through a minimum around $k = 13$, and finally increases slowly with k. For long k-mers, the critical threshold tends to 0.615(1) [9–12]; (iii) as results from (i) and (ii), percolation always occurs before jamming; (iv) the last statement was corroborated by Kondrat *et al.* [13], who demonstrated that any jammed configuration is a percolating state; and (iv) the problem belongs to the standard 2D random percolation universality class regardless of the size of k [14].

*antorami@unsl.edu.ar

With respect to triangular lattices, Budinski-Petković and Kozmidis-Luburić [15] studied the RSA kinetics of objects of various sizes and shapes deposited on a triangular array. In all cases, and by using numerical simulations for values of k ranging between 1 and 11, the authors reported an exponential decrease in $\theta_{j,k}$ with k. In Ref. [20], the calculations for straight rigid k-mers were extended up to $k = 128$. From $k \geqslant 12$, the jamming curve was successfully fitted by the function $\theta_{j,k} = 0.5976(5) + 1.268(30)/k - 3.61(34)/k^2$, being 0.5976(5) the limit coverage by very long depositing objects.

In Ref. [20], the percolation problem of irreversibly deposited linear k-mers on triangular lattices was also investigated. Using values of k between 2 and 256, the authors found that the percolation threshold $\theta_{c,k}$ shows a nonmonotonic behavior, with a minimum around $k = 13$. The decreasing tendency observed for shorter k-mers had already been described by Budinski-Petković *et al.* [16], who studied the problem for linear segments with values of k up to 20. Finally, in the range of k between 13 and 256, Perino *et al.* [20] reported an increasing trend in the percolation threshold. A similar behavior was observed for square lattices and k-mer size ranging between $k = 13$ and $k \approx 1024$. However, as mentioned above, extensive numerical simulations (up to $k = 2^{17}$) showed that the percolation threshold for linear k-mers on square lattices tends to a saturation value as $k \to \infty$ [12]. Accordingly, more simulations are necessary to obtain a definitive conclusion on the value of $\theta_{c,k\to\infty}$ for triangular lattices.

Despite over two decades of intensive research on jamming and percolation phenomena in 2D substrates, most studies have focused in the case of square [8–14] and triangular [15–20] lattices, and the problem of elongated k-mers irreversibly adsorbed on honeycomb lattices has not been investigated yet. In this context, the main objective of the present work is to study the jamming and percolation properties of linear rods on 2D honeycomb lattices. In the case of square and triangular lattices, the concept of straight rigid rod is trivial. Here, the depositing particle is a linear array of length k, maximizing the distance between first and last monomers in the chain. Extensive computer simulations (with $2 \leqslant k \leqslant 128$ and $24 \leqslant L/k \leqslant 80$), supplemented by finite-size scaling analysis, were carried out. The study allowed us to obtain the dependencies of the jamming coverage and percolation threshold on the size k. In addition, an exhaustive analysis of critical exponents and universality was performed. All of these quantities were reported for the first time in this paper.

This study is a natural continuation of earlier work on jamming and percolation in 2D lattices. In this framework, the structure of lattice space plays a fundamental role in determining the statistics of RSA states. Then, it is of theoretical interest to extend the existing research to systems with honeycomb symmetry. In addition, there is another reason why honeycomb lattices might be particularly interesting. From an experimental point of view, honeycomb lattices are intriguing systems, forming the structure of many natural and artificial objects [29–48]. Honeycomb lattices composed of carbon atoms form graphene sheets and carbon nanotubes [31–37]. The spontaneous formation of honeycomb structures has been observed in self-assembled layers of anthraquinone molecules on a Cu(111) surface [38,39]. Cells in epithelial sheets arrange themselves into honeycomb lattices [40]. Artificial honeycomb films have also been realized with different properties, such as photoelectric conversion [41], photocatalysis [42], antireflection [43], hydrophobicity [44], high mechanical strength [45], and cell adhesion [46–48].

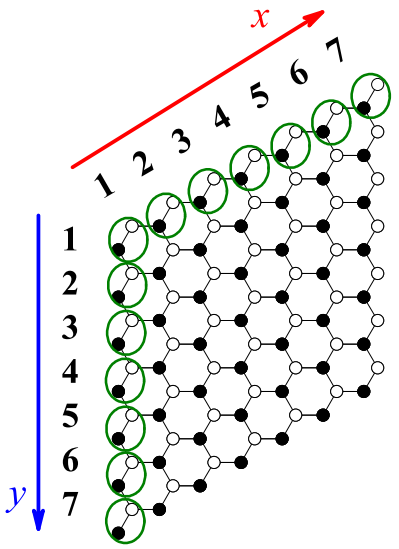

FIG. 1. Schematic representation of a rhombus-shaped honeycomb lattice with $L = 7$. Solid and open circles represent a and b sites, respectively.

The paper is organized as follows. The model and deposition kinetics are described in Sec. II. Percolation properties are studied in Sec. III. Finally, the conclusions are drawn in Sec. IV.

II. MODEL AND JAMMING PROPERTIES

Linear k-mers are deposited randomly, sequentially, and irreversibly on a 2D honeycomb lattice. In the computer simulations, a rhombus-shaped system of $M = 2 \times L \times L$ sites is used. As it is well-known, the honeycomb lattice is not a Bravais lattice and two types of sites (a and b) can be distinguished. See Fig. 1, where a rhombus-shaped honeycomb lattice with $L = 7$ is shown. Each a site (solid circle in Fig. 1) is connected to three b sites and each b site (open circle in Fig. 1) is connected to three a sites. In addition, the total number of $a(b)$ sites in the lattice is $M_a(M_b) = L \times L$. Accordingly, $M_a = M_b = M/2$.

The filling of the lattice with k-mers is carried out following the conventional RSA process [7]. It is performed with the following restrictions: (1) the k-mers contain k identical units and each one occupies a lattice site. Small adsorbates with spherical symmetry would correspond to the monomer limit ($k = 1$); (2) the distance between k-mer units is assumed in registry with the lattice constant l, and hence exactly k sites are occupied by a k-mer when deposited; (3) the incoming particles must not overlap with previously added objects; and (4) open boundary conditions are considered in both x and y directions. Under these conditions, the k-mers are forced to deposit inside the lattice (they are forbidden to cross the lattice edges).

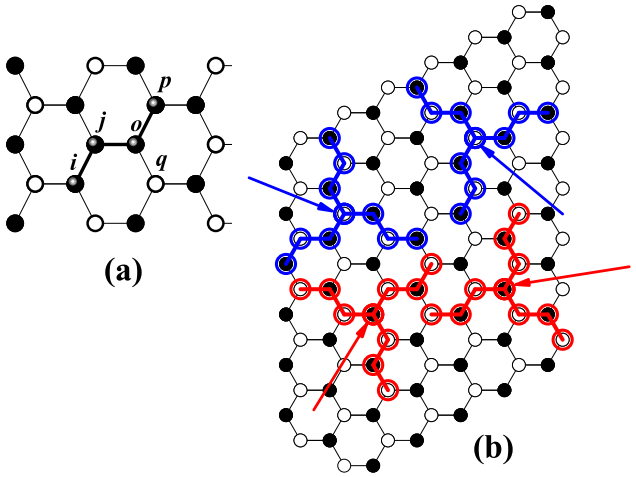

FIG. 2. (a) Linear tetramer adsorbed on a honeycomb lattice. Solid spheres represent tetramer units. (b) Available configurations for linear tetramers deposited on honeycomb lattices. In each case, an arrow denotes the initial site. As in Fig. 1, solid and open circles represent a and b sites, respectively.

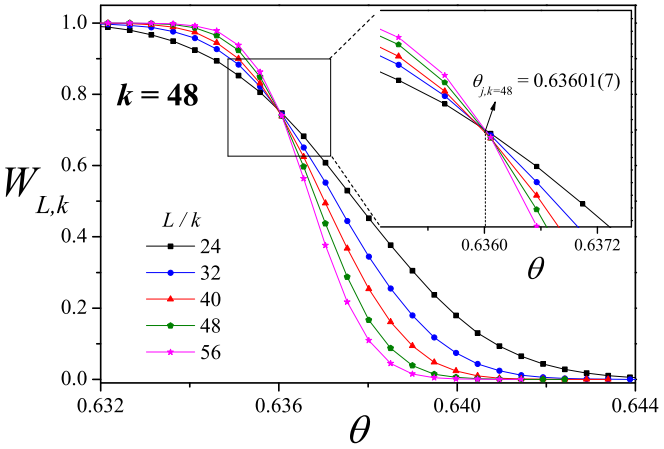

FIG. 3. Curves of $W_{L,k}(\theta)$ as a function of the fraction of occupied sites θ for $k = 48$ and different lattice sizes as indicated. Vertical dashed line denotes the jamming threshold in the thermodynamic limit: $\theta_{j,k=48} = 0.63601(7)$.

The concept of linear or straight rigid k-mer is trivial for square and triangular lattices [8–20], respectively. However, in a honeycomb lattice, the geometry does not allow the existence of a straight array of monomers. In this case, we call linear k-mer to a chain of adjacent monomers with the following sequence: once the first monomer is in place, the second monomer occupies one of the three nearest-neighbor of the first monomer. Third monomer occupies one of the two nearest-neighbor of the second monomer. i-esime monomer (for $i \geqslant 4$) occupies one of the two nearest-neighbor of the preceding monomer, which maximizes the distance between first monomer and i-esime monomer. This procedure allow us to place k monomers on a honeycomb lattice without creating an overlap.

Figure 2(a) illustrates the deposition process for a linear tetramer ($k = 4$) on a honeycomb lattice. Once first, second and third monomers were adsorbed in positions denoted as i, j, and o, respectively, there exist two possible positions for depositing the fourth monomer, p and q. To maximize the distance between the position of first and fourth monomers, site p is selected and site q is discarded. Following this procedure, 12 different configurations can be obtained for a linear k-mer with $k > 2$: 6 configurations have a type a site as the initial site, and 6 configurations have a type b site as the initial site. The 12 available sequences for linear tetramers on honeycomb lattices are shown in Fig. 2(b).

Then, the deposition process consists of the following steps, namely, (i) starting from an initially empty lattice; (ii) a given i site is randomly chosen; i site is the initial site [see Fig. 2(b)]; (iii) if the i site is empty, one of the six possible sequences for the linear k-mer is randomly chosen; (iv) if the $(k-1)$ selected sites in step (iii) are empty, then, a linear k-mer is deposited onto the lattice. Otherwise, the attempt is rejected. The procedure is repeated until a desired concentration $\theta = kN/M$ is reached (N is the number of the deposited k-mers).

The irreversible deposition of objects larger than a simple monomer (particle occupying one lattice site) involves the possibility of jamming. Namely, due to the blocking of the lattice by the already randomly adsorbed elements, the limiting or jamming coverage, $\theta_j = \theta(t \to \infty)$ is less than that corresponding to the close packing ($\theta_j < 1$). Note that $\theta(t)$ represents the fraction of lattice sites covered at time t by the deposited objects. Consequently, θ ranges from 0 to θ_j for objects occupying more than one site [7]. Our interest is in determining how the limiting concentration is modified when the size of the k-mer is increased.

To calculate the jamming coverage, it is useful to define the probability $W_{L,k}(\theta)$ that an $L \times L$ lattice reaches a coverage θ [49]. The subindex k in the probability function indicates that the coverage θ was reached after depositing objects of size k. In the simulations, the procedure to determine $W_{L,k}(\theta)$ consists of the following steps: (a) the construction of the L-lattice (initially empty) and (b) the deposition of objects on the lattice up to reach a particular jammed state at coverage θ_i. In the late step, the quantity $m_i(\theta)$ is calculated as

$$m_i(\theta) = \begin{cases} 1 & \text{for } \theta \leqslant \theta_i, \\ 0 & \text{for } \theta > \theta_i. \end{cases} \tag{1}$$

n runs of such two steps (a) and (b) are carried out for obtaining the number $m(\theta)$ of them for which a lattice reaches a coverage θ,

$$m(\theta) = \sum_{i=1}^{n} m_i(\theta). \tag{2}$$

Then, $W_{L,k}(\theta) = m(\theta)/n$ is defined and the procedure is repeated for different values of L and k. A set of $n = 10^5$ independent samples is numerically prepared for several values of the lattice size ($L/k = 24, 32, 40, 48, 56$). The L/k ratio is kept constant to prevent spurious effects due to the size k in comparison with the lattice linear size L.

In Fig. 3, the curves of probability for the different L/k values are shown for a typical case, $k = 48$. As mentioned in the previous paragraph, the simulations were performed for

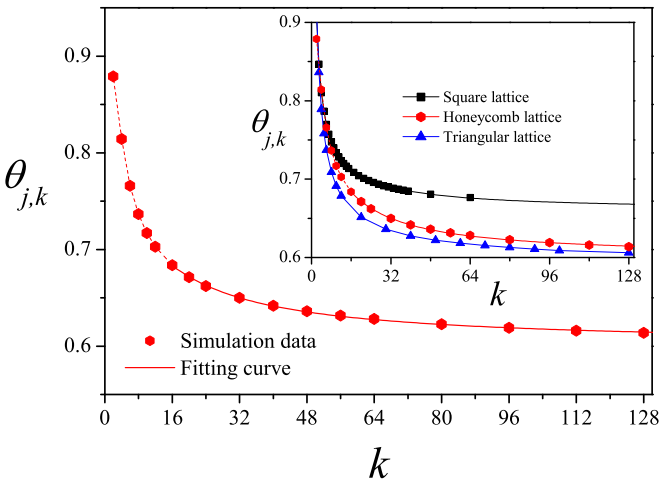

FIG. 4. Jamming coverage $\theta_{j,k}$ as a function of k for linear k-mers on honeycomb lattices with k between 2 and 128. Solid hexagons represent simulation results (the size of the points is larger than the corresponding error bars). The solid line corresponds to the fitting function as discussed in the text. Inset: The main curve in the figure is shown in comparison with the data of jamming coverage as a function of size k corresponding to (i) straight rigid k-mers on 2D square lattices (solid squares, Refs. [8,54]); and (ii) straight rigid k-mers on 2D triangular lattices (solid triangles, Ref. [20]).

lattice sizes ranging between $L/k = 24$ and $L/k = 56$. The curves $W_{L,k}(\theta)$ approach to the step function as L grows to infinity. Alternatively, for a finite value of L, the probability $W_{L,k}(\theta)$ varies continuously from 1 to 0, with a sharp fall around $\theta_{j,k}$. Even when the probabilities show a dependence on the system size, $W_{L,k}(\theta)$ is independent of the system size for $\theta = \theta_{j,k}$ [49]. Thus, the value of $\theta_{j,k}$ can be obtained from the crossing point of the curves of $W_{L,k}(\theta)$ for different lattice sizes. In the case of the figure, $\theta_{j,k=48} = 0.63601(7)$.

As has already been discussed in the literature [50,51], the use of different boundary conditions influences the behavior of the jamming properties. In this case, the use of open boundary conditions is responsible for the height of the crossing point $W_{L,k}(\theta_{j,k}) \approx 0.75$ observed in Fig. 3. As periodic boundary conditions are used, the value of the intersection point of the jamming probability curves is $W_{L,k}(\theta_{j,k}) \approx 0.5$ [49,52,53]. However, and independently of the considered boundary conditions (open or periodic), the methodology shown in Fig. 3 provides very accurate values of the jamming thresholds.

The procedure of Fig. 3 was repeated for k from 2 to 128, the results are presented in Fig. 4 and collected in Table I. From $k \geqslant 16$ the data have been fitted by the function $\theta_{j,k} = A + B/k + C/k^2$, as proposed in Refs. [8,20]; it is found that $A = 0.6007(6)$, $B = 1.84(5)$ and $C = -8.36(70)$. The fitting curve is included in Fig. 4 (solid line). The value of A represents the limit concentration by infinitely long k-mers: $A = \theta_{j,k\to\infty} = 0.6007(6)$.

The decreasing behavior of the jamming coverage with the size k towards an asymptotic limit value has been already observed in numerous systems. The cases of linear k-mers on 2D square [8], 2D triangular [20], and 3D cubic lattices [49], $k \times k$ tiles on 2D square [55] and 3D cubic lattices [53], and $k \times k \times k$ cubic objects on 3D cubic lattices [56], are examples of this. However, to the best of our knowledge, the case corresponding to honeycomb lattices has not been reported up to now.

TABLE I. Jamming coverages for different values of k.

k	$\theta_{j,k}$
2	0.87900(20)
4	0.81419(6)
6	0.76600(5)
8	0.73666(10)
10	0.71699(2)
12	0.70286(3)
16	0.68373(5)
20	0.67122(3)
24	0.66220(6)
32	0.64989(5)
40	0.64178(2)
48	0.63601(7)
56	0.63156(8)
64	0.62804(10)
80	0.62270(6)
96	0.61897(15)
112	0.61600(12)
128	0.61378(22)

In the inset of Fig. 4, the jamming curve corresponding to linear k-mers on honeycomb lattices is compared with similar data obtained previously for (i) straight rigid k-mers on 2D square lattices (solid squares, Refs. [8,54]); and (ii) straight rigid k-mers on 2D triangular lattices (solid triangles, Ref. [20]).

Two main conclusions can be drawn from the comparison in Fig. 4. First, the results obtained for honeycomb lattices are close to those reported for triangular lattices. This finding can be understood with the help of Fig. 2(b). There, it is possible to observe that, once a given site is chosen as an initial site, there are six k-tuples of adjacent sites available for deposition ($k > 2$). The same occurs for straight rigid k-mers on 2D triangular lattices, where the lattice connectivity is $c = 6$ (see Fig. 5). Then, for the case of linear k-mers deposited under the conditions described at the beginning of this section, the honeycomb lattices can be thought as lattices with an effective connectivity $c_{\text{eff}} = 6$. This property is responsible for the small differences observed between the jamming curves for honeycomb and triangular lattices.

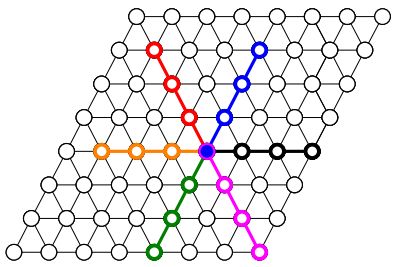

FIG. 5. Available configurations for straight rigid tetramers on triangular lattices (open circles joined by thick lines). The initial site is indicated by a solid circle.

Second, the saturation value $\theta_{j,k\to\infty} = 0.6007(6)$ for honeycomb lattices is less than the value $\theta_{j,k\to\infty} = 0.660(2)$ reported for linear k-mers on square lattices [8]. As discussed in the previous paragraph, the honeycomb lattice can be characterized by an effective connectivity $c_{\text{eff}} = 6$. Then, the obtained result indicates that the limiting coverage for infinitely long k-mers diminishes with increasing the lattice connectivity. A similar scenario has already been observed in previous work. Thus, $\theta_{j,k\to\infty} \approx 0.7475979$ (1D lattice, $c = 2$) [27]; $\theta_{j,k\to\infty} = 0.660(2)$ (2D square lattice, $c = 4$) [8,54]; and $\theta_{j,k\to\infty} = 0.5976(5)$ (2D triangular lattice, $c = 6$) [20].

III. PERCOLATION

Once the limiting concentrations $\theta_{j,k}$ are determined, the percolation properties are calculated using an standard simulation scheme [20,55]. An elemental simulation step consists of the following stages:

(1) We set L, k and a given lattice coverage θ.

(2) The sites are arranged in an $L \times L$ honeycomb lattice. At the starting configuration, all lattice sites are empty. Then, applying the filling process described in Sec. II, the lattice is covered up to the desired concentration θ is reached.

(3) The cluster analysis of the sample generated in stage (2) is performed. By employing the Hoshen-Kopelman algorithm [57] with open boundary conditions, the size of the largest cluster S_L is determined. In addition, the existence (or not) of a percolating cluster is established, according to the following criteria:

(a) X (along the x direction): the percolating cluster connects the left side to the right side of the lattice. See Fig. 1, and

(b) Y (along the y direction): the percolating cluster connects the bottom side to the top side of the lattice. See Fig. 1.

Other useful definitions for the finite-size analysis are:

(a) U (union): the percolating cluster spans from left to right *or* from bottom to top of the lattice, and

(b) I (intersection): the percolating cluster spans from left to right *and* from bottom to top of the lattice.

A total of m independent runs of (1)–(3) stages were carried out for each lattice side L, object size k, and concentration θ (ranging between 0 and $\theta_{j,k}$). A number m^i of samples (out of the total number m) presents a percolating cluster according to the $i \equiv \{X, Y, U, I\}$ criterion. Then, the corresponding percolation probability $R^i_{L,k}(\theta) = m^i/m$ can be defined. $R^i_{L,k}(\theta)$ ($i \equiv \{X, Y, U, I\}$) represents the probability that a lattice composed of $2L^2$ sites percolates at the concentration θ, according to the i criterion. It is also convenient to define the average probability $R^A_{L,k}(\theta) = [R^U_{L,k}(\theta) + R^I_{L,k}(\theta)]/2$.

The quantities related with the size of the largest cluster S_L, such as the order parameter P, the susceptibility χ and the reduced fourth-order cumulant U_L introduced by Binder [58], were also calculated:

$$P = \langle S_L \rangle / M, \tag{3}$$

$$\chi = \left[\langle S_L^2 \rangle - \langle S_L \rangle^2\right]/M, \tag{4}$$

and

$$U_L = 1 - \frac{\langle S_L^4 \rangle}{3\langle S_L^2 \rangle^2}, \tag{5}$$

where $\langle ... \rangle$ means an average over the m simulation runs. In the present work, we used $m = 10^5$ independent samples. In addition, for each value of L, k and θ, the effect of finite size was investigated by examining honeycomb lattices with $L/k = 48, 56, 64, 72, 80$. From this, finite-scaling theory can be used to determine the percolation threshold and the critical exponents with excellent accuracy.

The standard finite-size scaling theory [22,58–60] allows for various efficient routes to estimate the percolation threshold from simulation data. In the present paper, three procedures were applied, as described next.

Method I: The percolation thresholds are obtained from the crossing point of the curves of $R^i_{L,k}(\theta)$ for different values of L. These percolation probabilities, introduced by Yonezawa *et al.* [59,60], have been widely used in the literature. Percolation thresholds determined by Method I (and i criterion) will be denoted by $\theta^{\text{I},i}_{c,k}$.

Method II: A well-known property of the fourth-order Binder cumulants [Eq. (5)] is their independence on the system size at the critical point [58], in this case as $\theta = \theta_{c,k}$. Thus, plotting U_L for different linear lattice dimensions L yields an intersection point, which gives an accurate estimation of the percolation threshold in the infinite system. Percolation thresholds determined by Method II will be denoted by $\theta^{\text{II}}_{c,k}$.

Method III: The positions of the inflection points of the probabilities functions $R^i_{L,k}(\theta)$'s allow to obtain the effective percolation thresholds $\theta^i_{c,k}(L)$'s. Once the values of $\theta^i_{c,k}(L)$ are determined for all lattice sizes, a scaling analysis can be done to calculate the percolation threshold in the thermodynamic limit $\theta^i_{c,k}(\infty)$ [22,58–60]:

$$\theta^i_{c,k}(L) = \theta^i_{c,k}(\infty) + A^i L^{-1/\nu}, \qquad i \equiv \{X, Y, U, I, A\}, \tag{6}$$

where A^i is a nonuniversal constant and ν is the critical exponent of the correlation length. Some authors [61,62] have shown that even at the critical point (critical concentration when discussing percolation) there is a second length-scale. Within the precision of our simulation results, this second length-scale is not observed. From extrapolations it is possible to obtain $\theta^i_{c,k}(\infty)$ for the criteria I, A and U. Combining the three estimates for each case, the final values of $\theta_{c,k}(\infty)$ can be obtained. Additionally, the maximum of the differences between $|\theta^U_{c,k}(\infty) - \theta^A_{c,k}(\infty)|$ and $|\theta^I_{c,k}(\infty) - \theta^A_{c,k}(\infty)|$ gives the error bar for each determination of $\theta_{c,k}(\infty)$. Percolation thresholds determined by Method III will be denoted by $\theta^{\text{III}}_{c,k}$ [for simplicity we will drop the "(∞)"].

For a more precise application of Method III, it is useful to fit $R^i_{L,k}(\theta)$ with some approximating function. This procedure allows us to write the probability functions in terms of continuous values of concentration. Around the inflection point, $R^i_{L,k}(\theta)$ can be fitted by the error function because $dR^i_{L,k}(\theta)/d\theta$ is approximately a Gaussian function near the peak [59,60]. Then, fitting $dR^i_{L,k}(\theta)/d\theta$ with a Gaussian function is a good approximation for the purpose of locating its

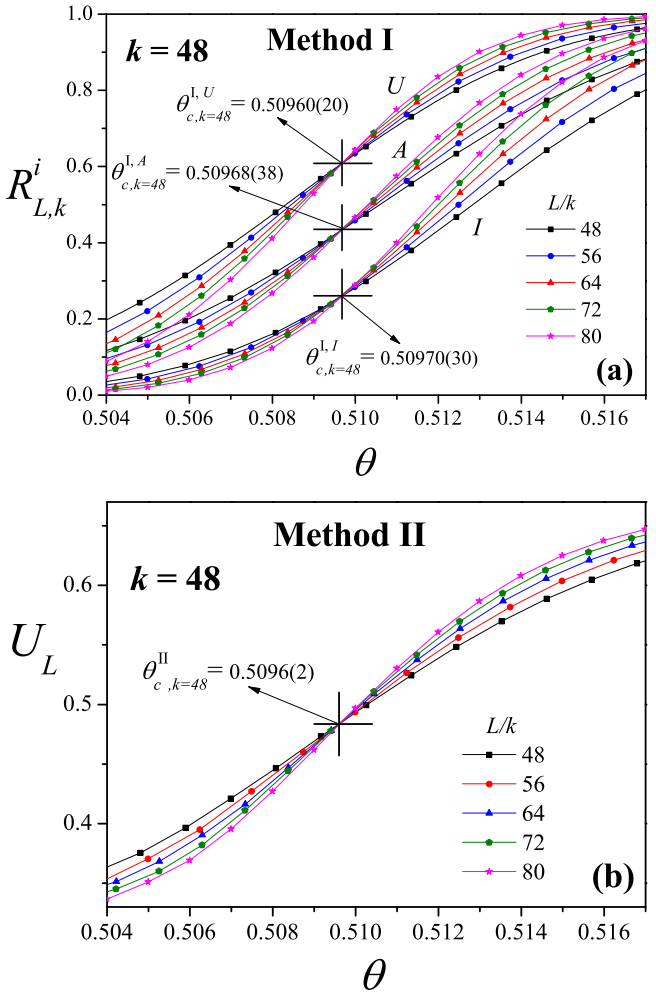

FIG. 6. (a) Method I. Fraction of percolating lattices $R^i_{L,k}(\theta)$ ($i \equiv \{U, I, A\}$) as a function of the concentration θ for $k = 48$ and different values of L/k: $L/k = 48$, squares; $L/k = 56$, circles; $L/k = 64$, triangles; $L/k = 72$, pentagons and $L/k = 80$, stars. The statistical errors are smaller than the symbol sizes. For each criterion, the curves cross each other in a very well-defined interval in the θ axis, which allows for a precise determination of the percolation threshold. In this case, $\theta^{I,A}_{c,k=48} = 0.50968(38)$; $\theta^{I,I}_{c,k=48} = 0.50970(30)$ and $\theta^{I,U}_{c,k=48} = 0.50960(20)$. (b) Method II. Curves of U_L vs. θ for $k = 48$ and different values of L/k [symbols are as in part (a)]. From their intersections one obtained $\theta^{II}_{c,k}$. In this case, $\theta^{II}_{c,k=48} = 0.5096(2)$.

maximum [63],

$$\frac{dR^i_{L,k}(\theta)}{d\theta} = \frac{1}{\sqrt{2\pi}\Delta^i_{L,k}} \exp\left\{-\frac{1}{2}\left[\frac{\theta - \theta^i_{c,k}(L)}{\Delta^i_{L,k}}\right]^2\right\},$$
$$i \equiv \{X, Y, U, I, A\}, \tag{7}$$

where the effective threshold $\theta^i_{c,k}(L)$ is the concentration at which the slope of $dR^i_{L,k}/d\theta$ is the largest and $\Delta^i_{L,k}$ is the standard deviation from $\theta^i_{L,k}(L)$.

For each value of k, Methods I–III were applied for obtaining the percolation threshold. A typical case is shown in Figs. 6(a) (Method I), 6(b) (Method II), and 7 (Method III). The data correspond to $k = 48$ and different values of L/k: $L/k = 48$, squares; $L/k = 56$, circles; $L/k = 64$, triangles; $L/k = 72$, pentagons and $L/k = 80$, stars.

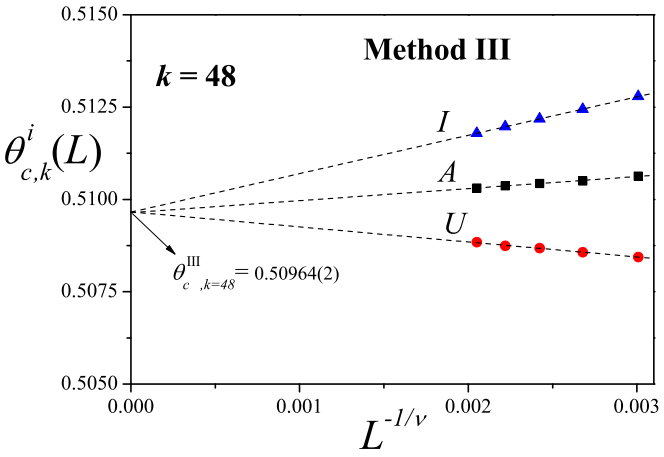

FIG. 7. Method III. Extrapolation of $\theta^i_{c,k}(L)$ towards the thermodynamic limit according to the theoretical prediction given by Eq. (6) with $\nu = 4/3$ (see discussion in the text). Triangles, squares and circles denote the values of $\theta^i_{c,k}(L)$ obtained by using the criteria I, A, and U, respectively. The resulting percolation threshold is $\theta^{III}_{c,k=48} = 0.50964(2)$.

In Fig. 6(a), the percolation probabilities $R^i_{L,k}(\theta)$ ($i \equiv \{U, I, A\}$) are plotted as a function of coverage θ. $R^i_{L,k}(\theta)$ curves vary between 0 and 1, and show an intersection point around the critical concentration. Even though the transition is never sharp for finite systems, the excellent quality of the simulation data allows for a very precise determination of the percolation threshold. In fact, the curves cross each other in a very well-defined interval in the θ axis. The center of this interval represents the percolation threshold ($\theta^i_{c,k}$) and the width of the interval is the error in the determination of $\theta^i_{c,k}$. In the case of Fig. 6, $\theta^{I,A}_{c,k=48} = 0.50968(38)$; $\theta^{I,I}_{c,k=48} = 0.50970(30)$; and $\theta^{I,U}_{c,k=48} = 0.50960(20)$.

Following a similar procedure as in Fig. 6(a), the percolation threshold can also be determined from the crossing point of the cumulant curves for different values of L. See Fig. 6(b). In this case, the value obtained is $\theta^{II}_{c,k=48} = 0.5096(2)$.

The application of Method III is depicted in Fig. 7. The figure shows the plots towards the thermodynamic limit of $\theta^i_{c,k}(L)$ according to Eq. (6) for $k = 48$. The critical exponent ν is taken equal to 4/3 for this analysis, since, as it will be shown below, the present model belongs to the 2D random percolation universality [22]. In this case, the value obtained was $\theta^{III}_{c,k=48} = 0.50964(2)$ [for simplicity we will drop the "(∞)"].

As it can be observed from Figs. 6 and 7, the five values obtained for the percolation threshold coincide within statistical errors. The procedure was repeated for k ranging between 2 and 128. The obtained results are compiled in Table II. Clearly, Method III (sixth column in Table II) provides the most accurate results for all values of k. Accordingly, for the rest of the paper we will use just one percolation threshold for each k-mer size $\theta_{c,k}$, being $\theta_{c,k} = \theta^{III}_{c,k}$.

The behavior of the percolation threshold as a function of k is shown in Fig. 8 (solid hexagons). As can be observed,

TABLE II. Percolation thresholds for different values of k.

k	$\theta_{c,k}^{\mathrm{I},A}$	$\theta_{c,k}^{\mathrm{I},I}$	$\theta_{c,k}^{\mathrm{I},U}$	$\theta_{c,k}^{\mathrm{II}}$	$\theta_{c,k}^{\mathrm{III}}$
2	0.69079(51)	0.69080(20)	0.69094(66)	0.6914(10)	0.69052(20)
4	0.63070(65)	0.63050(50)	0.63060(30)	0.6310(5)	0.63046(6)
6	0.59009(22)	0.59006(10)	0.59020(50)	0.5905(4)	0.59008(10)
8	0.56510(30)	0.56510(20)	0.56510(40)	0.5653(4)	0.56511(3)
10	0.54921(20)	0.54920(30)	0.54940(30)	0.5496(6)	0.54925(10)
12	0.53861(45)	0.53860(50)	0.53870(40)	0.5387(4)	0.53860(7)
16	0.52595(11)	0.52600(20)	0.52590(30)	0.5260(1)	0.52597(9)
20	0.51902(42)	0.51910(60)	0.51910(50)	0.5192(6)	0.51911(10)
24	0.51498(20)	0.51500(20)	0.51500(30)	0.5150(8)	0.51496(7)
32	0.51116(21)	0.51110(20)	0.51120(40)	0.5111(4)	0.51116(10)
40	0.50986(4)	0.50980(30)	0.50990(10)	0.5098(4)	0.50984(5)
48	0.50968(38)	0.50970(30)	0.50960(20)	0.5096(2)	0.50964(2)
56	0.50998(12)	0.51000(20)	0.51000(20)	0.5098(2)	0.50993(6)
64	0.51038(25)	0.51036(36)	0.51041(40)	0.5103(3)	0.51037(8)
80	0.51186(6)	0.51180(20)	0.51190(18)	0.5115(4)	0.51178(3)
96	0.51338(18)	0.51333(20)	0.51342(28)	0.5132(3)	0.51337(15)
112	0.51470(50)	0.51433(27)	0.51444(22)	0.5145(5)	0.51472(11)
128	0.51623(5)	0.51625(18)	0.51637(17)	0.5160(6)	0.51618(4)

a nonmonotonic size dependence is found for $\theta_{c,k}$, which decreases in the range $2 \leqslant k < 48$, goes through a minimum around $k = 48$, and increases smoothly from $k = 48$ up to the largest studied value of $k = 128$. In the inset of Fig. 8, the curve in the main figure (solid hexagons), is compared with the data of percolation threshold as a function of size k corresponding to (i) straight rigid k-mers on 2D square lattices (solid squares, Ref. [12]); and (ii) straight rigid k-mers on 2D triangular lattices (solid triangles, Ref. [20]).

In the case of honeycomb lattices, the minimum observed in the percolation curve is less pronounced and shifted towards higher values of the size k, with respect to the minima obtained for square and triangular lattices. In addition, in the range of values studied ($2 \leqslant k \leqslant 128$), the percolation curve of honeycomb lattices remains above the percolation curves corresponding to square and triangular lattices. This behavior is expected given the coordination number of the three lattices. As has been demonstrated in numerous studies [22,64–67], percolation threshold varies inversely with the number of connections per site (bond). A prototype lattice is a Cayley tree (Bethe lattice), where the percolation threshold has been solved exactly to yield $p_c = 1/(z-1)$ with z neighbours for every site [22,64].

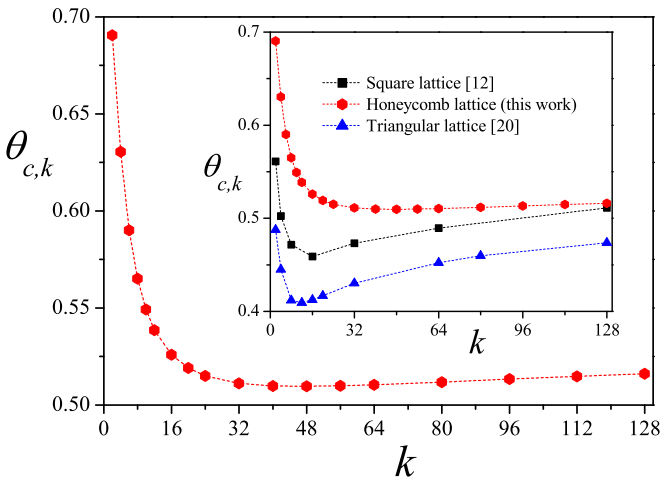

FIG. 8. Percolation threshold as a function of k for linear k-mers on honeycomb lattices. Inset: The main curve is shown in comparison with the data of percolation threshold as a function of size k corresponding to (i) straight rigid k-mers on 2D square lattices (solid squares) [12]; and (ii) straight rigid k-mers on 2D triangular lattices (solid triangles) [20]. Short-dashed lines are included as a guide to the eye.

As mentioned in Sec. I, a saturation value of the percolation threshold was found for infinitely long k-mers deposited on square lattices. Based in a very efficient parallel algorithm, Slutskii *et al.* [12] studied the problem of large linear k-mers (up to $k = 2^{17}$) on a square lattice. The authors reported that $\theta_{c,k} = 0.615(1)$ as k tends to infinite. This finding, along with the very slow increase of $\theta_{c,k}$ with k ($k > 48$) observed for honeycomb lattices, would indicate that square and honeycomb percolation curves intersect at some point $k > 128$. However, more extensive simulations are necessary to confirm this observation, and to obtain direct confirmation of the behavior of $\theta_{c,k}$ for infinitely long k-mers. This is beyond our current computational capabilities.

In the case of percolation of straight rigid k-mers on square and triangular lattices, it was found that the phase transition occurring in the system belongs to the 2D random percolation universality class theory [14,20]. Since there is no similar report for the case of honeycomb lattices, the main objective in what follows is to perform a detailed study of the critical exponents ν, β, and γ to determine the universality class of the percolation problem of linear k-mers on honeycomb lattices.

The analysis will be carried out by means of finite-size scaling theory [22,58–60]. The technique implies the

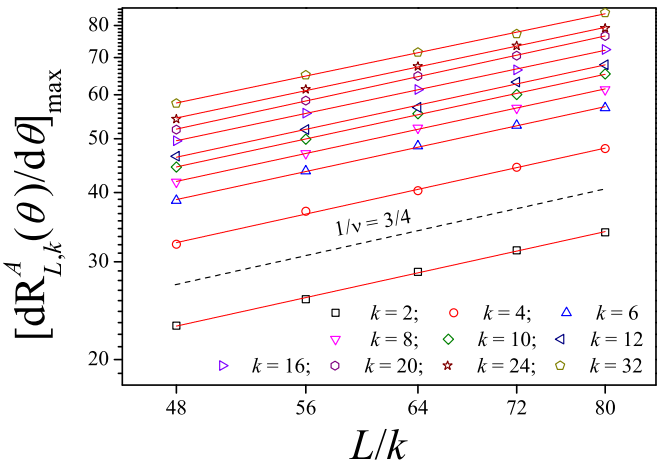

FIG. 9. Log-log plot of $[dR^A_{L,k}(\theta)/d\theta]_{\max}$ as a function of L/k for different values of k as indicated. According to Eq. (12) the slope of each line corresponds to $1/\nu = 3/4$.

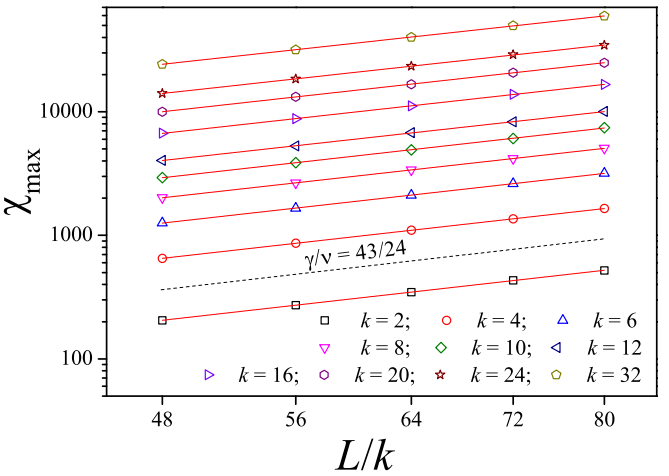

FIG. 11. Log-log plot of $\chi_{\max}$ as a function of L/k for the same cases reported in Fig. 9. According to Eq. (14), the slope of each curve corresponds to $\gamma/\nu = 43/24$.

following behavior of $R^i_{L,k}(\theta)$, $U_L(\theta)$, $P(\theta)$ and $\chi(\theta)$ at criticality,

$$R^i_{L,k}(\theta) = \overline{R^i_k}[(\theta - \theta_{c,k})L^{1/\nu}], \tag{8}$$

$$U_L(\theta) = \overline{U}[(\theta - \theta_{c,k})L^{1/\nu}], \tag{9}$$

$$P(\theta) = L^{-\beta/\nu}\overline{P}[|\theta - \theta_{c,k}|L^{1/\nu}], \tag{10}$$

and

$$\chi(\theta) = L^{\gamma/\nu}\overline{\chi}[(\theta - \theta_{c,k})L^{1/\nu}], \tag{11}$$

where $\overline{R^i_k}$, $\overline{U}$, $\overline{\chi}$, and $\overline{P}$ are the corresponding scaling functions.

We start with the calculation of the critical exponent ν. This quantity can be determined from the maximum of the derivatives of the function in Eqs. (8) and (9). Thus,

$$\left[\frac{dR^i_{L,k}(\theta)}{d\theta}\right]_{\max} \propto L^{1/\nu}, \quad \text{and} \quad \left[\frac{dU_L(\theta)}{d\theta}\right]_{\max} \propto L^{1/\nu}. \tag{12}$$

By plotting $[dR^i_{L,k}(\theta)/d\theta]_{\max}$ and $[dU_L(\theta)/d\theta]_{\max}$ as a function of L/k in log-log scale, the slopes of the curves will correspond to $1/\nu$. As an example, Fig. 9 shows the results obtained for $[dR^A_{L,k}(\theta)/d\theta]_{\max}$ and $2 \leqslant k \leqslant 32$. The slopes of the curves corresponds to $1/\nu$ and, as can be observed, remain constant (and close to 3/4) for all studied cases. The procedure was performed for $R^i_{L,k}(\theta)$ ($i \equiv \{U, I, A\}$), $U_L(\theta)$ $P(\theta)$, and k ranging between 2 and 128. The results are shown in Fig. 12 (solid triangles) and compiled in Table III. The value of ν in each point (corresponding to a given value of k) was calculated by combining the four estimates from R^A, R^I, R^U, and U_L.

However, a standard way to extract the critical ratios β/ν and γ/ν is to study the scaling behavior of the maximum of the derivative of $P(\theta)$ [Eq. (10)] and the maximum of the susceptibility $\chi(\theta)$ [Eq. (11)],

$$\left[\frac{dP(\theta)}{d\theta}\right]_{\max} \propto L^{(1-\beta)/\nu}, \tag{13}$$

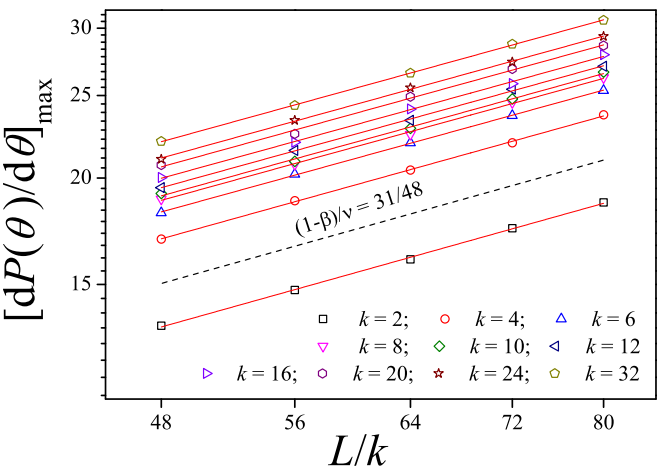

FIG. 10. Log-log plot of $[dP(\theta)/d\theta]_{\max}$ as a function of L/k for the same cases reported in Fig. 9. According to Eq. (13), the slope of each curve corresponds to $(1 - \beta)/\nu = 31/48$.

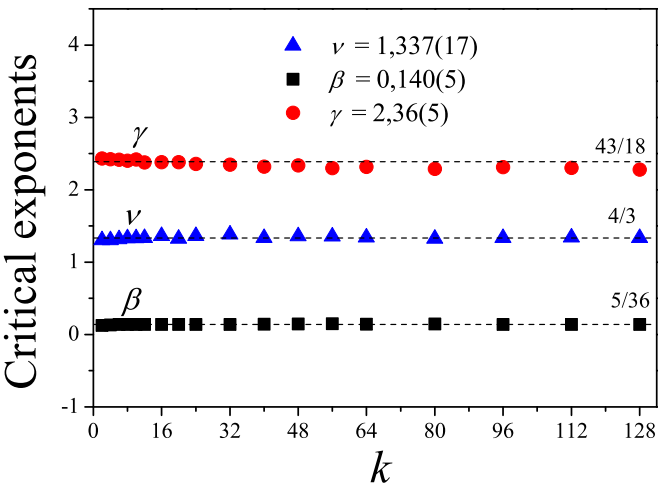

FIG. 12. Critical exponents ν (triangles), β (squares), and γ (circles) as a function of k. The reference values corresponding to 2D random percolation are shown as solid horizontal lines.

TABLE III. Critical exponents ν, β, and γ for different values of k.

k	ν	β	γ
2	1.304(22)	0.127(13)	2.432(8)
4	1.304(36)	0.133(12)	2.421(5)
6	1.317(17)	0.140(7)	2.416(9)
8	1.332(16)	0.139(17)	2.403(7)
10	1.330(16)	0.141(19)	2.418(13)
12	1.334(30)	0.140(24)	2.378(11)
16	1.362(34)	0.140(16)	2.382(8)
20	1.323(11)	0.140(24)	2.383(9)
24	1.359(32)	0.139(12)	2.356(13)
32	1.381(49)	0.140(5)	2.349(9)
40	1.335(25)	0.142(8)	2.320(13)
48	1.357(28)	0.147(13)	2.338(7)
56	1.354(27)	0.149(13)	2.300(11)
64	1.339(27)	0.143(17)	2.318(13)
80	1.325(23)	0.145(8)	2.288(13)
96	1.335(34)	0.141(13)	2.314(13)
112	1.339(20)	0.140(11)	2.304(12)
128	1.335(28)	0.138(8)	2.277(12)

and

$$\chi_{\max} \propto L^{\gamma/\nu}. \tag{14}$$

When Eqs. (13) and (14) are represented in a log-log scale, the slopes of the corresponding curves are $(1-\beta)/\nu$ and γ/ν, respectively. This procedure is shown in Figs. 10 and 11 for the same cases studied in Fig. 9. The obtained values of the slopes are consistent with $(1-\beta)/\nu = 31/48$ (Fig. 10) and $\gamma/\nu = 43/24$ (Fig. 11). A similar study was done for k ranging between 2 and 128. The results are shown in Fig. 12 [β (squares) and γ (circles)] and collected in Table III.

Figure 12 summarizes the results given in Figs. 9–11 (and data not shown for brevity). In all cases, the values obtained for ν, β, and γ coincide, within numerical errors, with the exact values of the critical exponents for the 2D ordinary percolation, namely, $\nu = 4/3$, $\beta = 5/36$, and $\gamma = 43/18$ [22]. In the figure, these reference values are shown as solid horizontal lines. By averaging on all the k studied sizes, the following values were obtained: $\nu = 1.337(17)$, $\beta = 0.140(5)$, and $\gamma = 2.36(5)$.

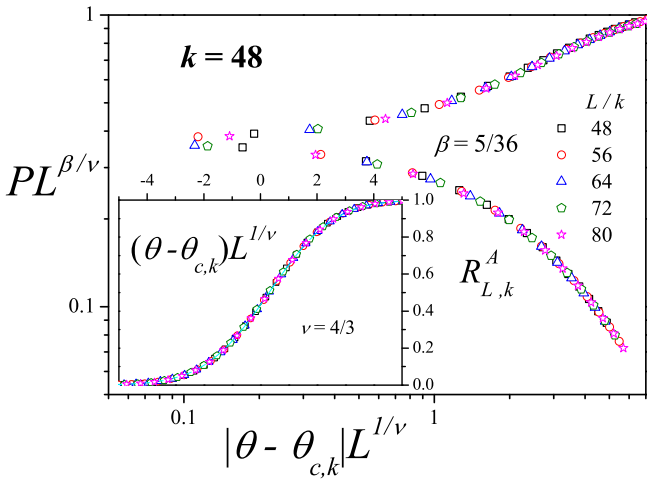

FIG. 13. Data collapse of the order parameter, $P(\theta)L^{\beta/\nu}$ vs. $|\theta-\theta_{c,k}|L^{1/\nu}$, and of the percolation probabilities, $R^i_{L,k}(\theta)$ vs. $(\theta-\theta_{c,k})L^{1/\nu}$ (inset) for the case $k=48$. The plots were made using $\theta_{c,k=48} = 0.50964(2)$ (see Table II, sixth column) and exact 2D random percolation exponents $\nu = 4/3$ and $\beta = 5/36$.

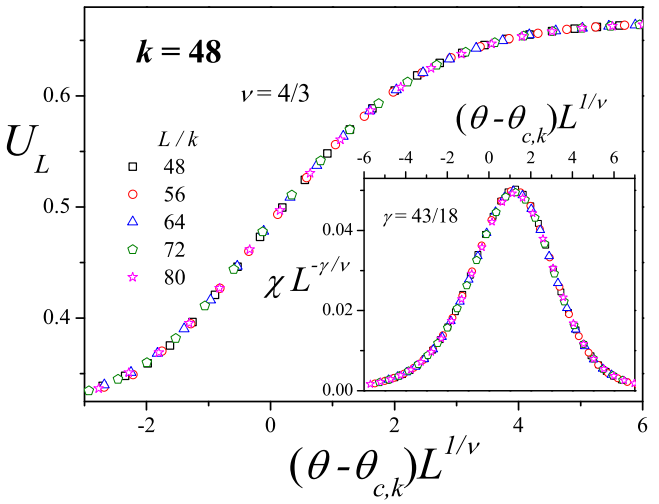

FIG. 14. Data collapse of the cumulant, $U_L(\theta)$ vs. $(\theta-\theta_{c,k})L^{1/\nu}$, and of the susceptibility, $\chi(\theta)L^{-\gamma/\nu}$ vs. $(\theta-\theta_{c,k})L^{1/\nu}$ (inset) for the case $k=48$. The plots were made using $\theta_{c,k=48} = 0.50964(2)$ (see Table II, sixth column) and exact 2D random percolation exponents $\nu = 4/3$ and $\gamma = 43/18$.

It is also interesting to test the data collapse scaling of $R^i_{L,k}(\theta)$, $U_L(\theta)$, $P(\theta)$, and $\chi(\theta)$. This can be carried out by plotting $R^i_{L,k}(\theta)$ vs. $(\theta-\theta_{c,k})L^{1/\nu}$, $U_L(\theta)$ vs. $(\theta-\theta_{c,k})L^{1/\nu}$, $P(\theta)L^{\beta/\nu}$ vs. $|\theta-\theta_{c,k}|L^{1/\nu}$, and $\chi(\theta)L^{-\gamma/\nu}$ vs. $(\theta-\theta_{c,k})L^{1/\nu}$, with an adequate choice of the critical parameters ν, β, γ, and $\theta_{c,k}$. An example is shown in Figs. 13 and 14, where the case $k=48$ is analyzed. Excellent collapses were achieved using the exact 2D random percolation critical exponents ($\nu = 4/3$, $\beta = 5/36$, and $\gamma = 43/18$) and $\theta_{c,k=48} = 0.50964(2)$ (see Table II, sixth column).

The study in Figs. 13 and 14 was successfully repeated for all the studied values of k. Our findings confirm that this percolation phase transition, occurring on honeycomb lattices, belongs to the same universality class as the 2D random percolation, regardless of the size k considered.

IV. CONCLUSIONS

Jamming and percolation behavior of linear k-mers deposited onto a honeycomb lattice have been studied by extensive numerical simulations supplemented by finite-size scaling theory. The linear k-mer is modeled as k interaction centers at a fixed separation, which is equal to the lattice constant. Thus, k sites are occupied by a k-mer when adsorbed onto the surface. Since the geometry of the honeycomb lattice does not allow the existence of a straight rigid chain of monomers, we call linear k-mer to an array of k adjacent monomers, maximizing the distance between first and last monomers in the array. The elongated objects are deposited by following the standard random sequential adsorption (RSA) process.

The simulations were performed for k-mer sizes ranging between 2 and 128, and $L \times L$ lattices with $24 \leqslant L/k \leqslant 80$. According to the present study, the critical behavior of the system is characterized by the following properties:

(1) The jamming coverage dependence on the particle size k follows a decreasing law: $\theta_{j,k} = 0.6007(6) + 1.84(5)/k - 8.36(70)/k^2$, being $\theta_{j,k\to\infty} = 0.6007(6)$ the limit value for infinitely long k-mers.

(2) According to the proposed deposition mechanism, once a given site is chosen as an initial site, there are six k-tuples (with $k > 2$) of adjacent sites available for deposition. This fact allows us to define an effective connectivity $c_{\text{eff}} = 6$, characterizing the jamming properties of the present model. Then, the comparison with previous research indicates that the limiting coverage for infinitely long k-mers diminishes with increasing the lattice connectivity: $\theta_{j,k\to\infty} \approx 0.7475979$ (1D lattice, $c = 2$) [27]; $\theta_{j,k\to\infty} = 0.660(2)$ (2D square lattice, $c = 4$) [8,54]; $\theta_{j,k\to\infty} = 0.5976(5)$ (2D triangular lattice, $c = 6$) [20] and $\theta_{j,k\to\infty} = 0.6007(6)$ (2D honeycomb lattice, $c_{eff} = 6$) in this work. The observed similarities between triangular and honeycomb symmetries can also be understood from the concept of effective connectivity.

(3) The percolation threshold exhibits a nonmonotonous behavior as a function of the k: $\theta_{c,k}$ decreases for small particles sizes, passes through a minimum around $k = 48$, and finally increases slowly for large segments. A similar nonmonotonic dependence with k had already been reported for square [12] and triangular [20] lattices. However, the functionality of $\theta_{c,k}$ with k is reported here for the first time in a honeycomb geometry.

(4) The comparison with previous studies for percolation of straight rigid k-mers on square [12]) and triangular [20] lattices indicates that: (i) in the range $2 \leqslant k \leqslant 128$, the percolation curve of honeycomb lattices remains above the percolation curves corresponding to square and triangular lattices; and (ii) in the case of honeycomb lattices, the minimum observed in the percolation curve is less pronounced and shifted towards higher values of the size k, with respect to the minima obtained for square and triangular lattices. More simulations are required to establish the definitive tendency of $\theta_{c,k}$ for straight rigid k-mers.

(5) Given a fixed value of k, percolation always occurs before jamming ($\theta_{c,k} < \theta_{j,k}$) and, consequently, the model presents percolation phase transition in all the k-space.

(6) The obtained values of the critical exponents $\nu = 1.337(17)$, $\beta = 0.140(5)$ and $\gamma = 2.36(5)$ clearly indicate that the observed percolation phase transition belongs to the universality class of the 2D standard percolation regardless of the value of k considered.

(7) Very recent studies from our group, still in progress [68], indicate that $\theta_{c,k} + \theta^i_{c,k} = 1$ for triangular lattices, where $\theta_{c,k}$ and $\theta^i_{c,k}$ represent the standard [20] and inverse [69] percolation thresholds for straight rigid k-mers, respectively. The observed complementarity between standard and inverse percolation thresholds is a distinctive footprint of the triangular geometry, and is not valid for honeycomb lattices [71]. This finding shows clearly that jamming and percolation problems on honeycomb lattices provide nontrivial physics, and their results cannot be derived from those previously obtained for triangular lattices.

ACKNOWLEDGMENTS

This work was supported in part by CONICET (Argentina) under Project No. PIP 112-201101-00615 and Universidad Nacional de San Luis (Argentina) under Project No. 03-0816. The numerical work were done using the BACO parallel cluster [72] located at Instituto de Física Aplicada, Universidad Nacional de San Luis-CONICET, San Luis, Argentina.

[1] J. J. Ramsden, Phys. Rev. Lett. **71**, 295 (1993).
[2] P. R. Van Tassel, L. Guemouri, J. J. Ramsden, G. Tarjus, P. Viot, and J. Talbot, J. Colloid Interface Sci. **207**, 317 (1998).
[3] M. Rabe, D. Verdes, and S. Seeger, Adv. Colloid Interface Sci. **162**, 87 (2011).
[4] L. Fingold and J. T. Donnell, Nature **278**, 443 (1979).
[5] Z. Adamczyk, T. Babros, J. Czarnecki, and T. G. M. van de Ven, Adv. Colloid Interface Sci. **19**, 183 (1983).
[6] V. Privman, H. L. Frisch, N. Ryde, and E. Matijvević, J. Chem. Soc. Faraday Trans. **87**, 1371 (1991).
[7] J. W. Evans, Rev. Mod. Phys. **65**, 1281 (1993).
[8] B. Bonnier, M. Hontebeyrie, Y. Leroyer, C. Meyers, and E. Pommiers, Phys. Rev. E **49**, 305 (1994).
[9] Y. Leroyer and E. Pommiers, Phys. Rev. B **50**, 2795 (1994).
[10] G. Kondrat and A. Pekalski, Phys. Rev. E **63**, 051108 (2001).
[11] Y. Y. Tarasevich, N. I. Lebovka, and V. V. Laptev, Phys. Rev. E **86**, 061116 (2012).
[12] M. G. Slutskii, L. Y. Barash, and Y. Y. Tarasevich, Phys. Rev. E **98**, 062130 (2018).
[13] G. Kondrat, Z. Koza, and P. Brzeski, Phys. Rev. E **96**, 022154 (2017).
[14] V. Cornette, A. J. Ramirez-Pastor, and F. Nieto, Eur. Phys. J. B **36**, 391 (2003).
[15] Lj. Budinski-Petković and U. Kozmidis-Luburić, Phys. Rev. E **56**, 6904 (1997).
[16] Lj. Budinski-Petković, I. Lončarević, M. Petković, Z. M. Jakšić, and S. B. Vrhovac, Phys. Rev. E **85**, 061117 (2012).
[17] Lj. Budinski-Petković, I. Lončarević, Z. M. Jakšić, S. B. Vrhovac, and N. M. Švrakić, Phys. Rev. E **84**, 051601 (2011).
[18] Lj. Budinski-Petković, I. Lončarević, Z. M. Jakšić, and S. B. Vrhovac, J. Stat. Mech. (2016) 053101.
[19] Lj. Budinski-Petković, I. Lončarević, D. Dujak, A. Karać, J. R. Šćepanović, Z. M. Jakšić, and S. B. Vrhovac, Phys. Rev. E **95**, 022114 (2017).
[20] E. J. Perino, D. A. Matoz-Fernandez, P. M. Pasinetti, and A. J. Ramirez-Pastor, J. Stat. Mech. (2017) 073206.
[21] M. Sahimi, *Applications of Percolation Theory* (Taylor & Francis, London, 1992).
[22] D. Stauffer and A. Aharony, *Introduction to Percolation Theory* (Taylor & Francis, London, 1994).
[23] G. Grimmett, *Percolation* (Springer-Verlag, Berlin, 1999).
[24] B. Bollobás and O. Riordan, *Percolation* (Cambridge University Press, New York, 2006).

[25] P. J. Flory, J. Am. Chem. Soc. **61**, 1518 (1939).

[26] A. Rényi, Sel. Transl. Math. Stat. Probab. **4**, 203 (1963) [translation from Magyar Tud. Akad. Mat. Kutató Int. Közl. **3**, 109 (1958)].

[27] P. L. Krapivsky, S. Redner, and E. Ben-Naim, *A Kinetic View of Statistical Physics* (Cambridge University Press, Cambridge, UK, 2010).

[28] A. Cadilhe, N. A. M. Araújo, and V. Privman, J. Phys.: Condens. Matter **19**, 065124 (2007).

[29] M. A. Spencer and R. M. Ziff, Phys. Rev. E **93**, 042132 (2016).

[30] Y. Chen, Y. Xie, Y. Gao, P.-Y. Chang, S. Zhang, and D. Vanderbilt, Phys. Rev. Mater. **2**, 044205 (2018).

[31] K. S. Novoselov, A. K. Geim, S. V. Morozov, D. Jiang, M. I. Katsnelson, I. V. Grigorieva, S. V. Dubonos, and A. A. Firsov, Nature **438**, 197 (2005).

[32] K. S. Novoselov, Z. Jiang, Y. Zhang, S. V. Morozov, H. L. Stormer, U. Zeitler, J. C. Maan, G. S. Boebinger, P. Kim, and A. K. Geim, Science **315**, 1379 (2007).

[33] M. I. Katsnelson, *Graphene: Carbon in Two Dimensions* (Cambridge University Press, Cambridge, UK, 2012).

[34] R. Saito, G. Dresselhaus, and M. S. Dresselhaus, *Physical Properties of Carbon Nanotubes* (Imperial College Press, London, UK, 1998).

[35] A. J. Phares, D. W. Grumbine, Jr., and F. J. Wunderlich, Langmuir **23**, 558 (2007).

[36] A. J. Phares, D. W. Grumbine Jr., and F. J. Wunderlich, Langmuir **26**, 10750 (2010).

[37] A. J. Phares, Langmuir **27**, 8105 (2011).

[38] G. Pawin, K. L. Wong, K.-Y. Kwon, and L. Bartels, Science **313**, 961 (2006).

[39] K. Kim and T. L. Einstein, Phys. Rev. B **83**, 245414 (2011).

[40] A. G. Fletcher, M. Osterfield, R. E. Baker, and S. Y. Shvartsman, Biophys. J. **106**, 2291 (2014).

[41] L. P. Heng, J. Zhai, Y. Zhao, J. J. Xu, X. L. Sheng, and L. Jiang, ChemPhysChem **7**, 2520 (2006).

[42] K. Kon, C. N. Brauer, K. Hidaka, H. G. Lohmannsroben, and O. Karthaus, Langmuir **26**, 12173 (2010).

[43] M. S. Park and J. K. Kim, Langmuir **21**, 11404 (2005).

[44] P. H. Tung, S. W. Kuo, K. U. Jeong, S. Z. D. Cheng, C. F. Huang, and F. C. Chang, Macromol. Rapid Commun. **28**, 271 (2007).

[45] X. Xu, L. P. Heng, X. J. Zhao, J. Ma, L. Lin, and L. J. Jiang, Mater. Chem. **22**, 10883 (2012).

[46] X. F. Li, Y. Wang, L. Zhang, S. X. Tan, X. L. Yu, N. Zhao, G. Q. Chen, and J. Xu, J. Colloid Interface Sci. **350**, 253 (2010).

[47] T. Nishikawa, M. Nonomura, K. Arai, J. Hayashi, T. Sawadaishi, Y. Nishiura, M. Hara, and M. Shimomura, Langmuir **19**, 6193 (2003).

[48] L. Heng, R. Hu, S. Chen, M. Li, L. Jiang, and B. Z. Tang, Langmuir **29**, 14947 (2013).

[49] G. D. García, F. O. Sanchez-Varretti, P. M. Centres, and A. J. Ramirez-Pastor, Physica A **436**, 558 (2015).

[50] M. Cieśla and R. M. Ziff, J. Stat. Mech. (2018) 043302.

[51] N. Vandewalle, S. Galam, and M. Kramer, Eur. Phys. J. B **14**, 407 (2000).

[52] P. M. Pasinetti, L. S. Ramirez, P. M. Centres, A. J. Ramirez-Pastor, and G. A. Cwilich, Phys. Rev. E **100**, 052114 (2019).

[53] P. M. Pasinetti, P. M. Centres, and A. J. Ramirez-Pastor, J. Stat. Mech. (2019) 103204.

[54] M. Dolz, F. Nieto, and A. J. Ramirez-Pastor, Phys. Rev. E **72**, 066129 (2005).

[55] A. J. Ramirez-Pastor, P. M. Centres, E. E. Vogel, and J. F. Valdés, Phys. Rev. E **99**, 042131 (2019).

[56] A. C. Buchini Labayen, P. M. Centres, P. M. Pasinetti, and A. J. Ramirez-Pastor, Phys. Rev. E **100**, 022136 (2019).

[57] J. Hoshen and R. Kopelman, Phys. Rev. B **14**, 3438 (1976).

[58] K. Binder, Rep. Prog. Phys. **60**, 488 (1997).

[59] F. Yonezawa, S. Sakamoto, and M. Hori, Phys. Rev. B **40**, 636 (1989).

[60] F. Yonezawa, S. Sakamoto, and M. Hori, Phys. Rev. B **40**, 650 (1989).

[61] G. I. Barenblatt, *Scaling, Self-similarity, and Intermediate Asymptotics* (Cambridge University Press, Cambridge, 1996).

[62] N. Goldenfeld, *Lectures on Phase Transitions and the Renormalization Group* (Addison-Wesley, Reading, MA, 1992).

[63] M. E. J. Newman and R. M. Ziff, Phys. Rev. Lett. **85**, 4104 (2000).

[64] M. E. Fisher and J. W. Essam, J. Math. Phys. **2**, 609 (1961).

[65] S. Galam and A. Mauger, Physica A **205**, 502 (1994).

[66] S. Galam and A. Mauger, Phys. Rev. E **53**, 2177 (1996).

[67] S. Galam and A. Mauger, Phys. Rev. E **56**, 322 (1997).

[68] L. S. Ramirez, P. M. Pasinetti, W. Lebrecht, and A. J. Ramirez-Pastor, Standard and inverse site percolation of straight rigid rods on triangular lattices: isotropic and nematic deposition (unpublished).

[69] L. S. Ramirez, P. M. Centres, and A. J. Ramirez-Pastor, J. Stat. Mech. (2017) 113204.

[70] L. S. Ramirez, P. M. Centres, A. J. Ramirez-Pastor, and W. Lebrecht, J. Stat. Mech. (2019) 113205.

[71] In the simplest case, $\theta_{c,k=2} \approx 0.69052$ (this work) and $\theta^i_{c,k=2} \approx 0.6366$ [70] for dimers on honeycomb lattices. Clearly, $\theta_{c,k=2} + \theta^i_{c,k=2} \neq 1$.

[72] Available at http://cluster_infap.unsl.edu.ar/wordpress.